DEVELOPMENT AND INITIAL HOVER TESTING OF THE MACH SCALED ROTOR TEST RIG MERIT

Verena Heuschneider * Florian Berghammer † Tobias Pflumm ‡ Manfred Hajek §

Institute of Helicopter Technology
Technical University of Munich, 80333 Munich, Germany

Abstract
The first part of this paper shows the development of the rotor test rig MERIT, designed and built at the Institute of Helicopter Technology, Technical University of Munich, Germany. It includes insight into mechanical component design, such as the rotor head, rotor blade, blade attachment, and swashplate as well as the measurement and data acquisition system architecture in the rotating and stationary frames with regard to the most restrictive design target, which is dynamic stall investigation in forward flight conditions. Test results show that the critical components' tensile strengths and eigenfrequencies meet the requirements. Furthermore, calibration results for the rotor load measuring cells are given. The second part focuses on hover tests, displaying the AREA rotor´s polar measurement results for power and thrust up to 12° collective pitch and at 550 to 800rpm. A comparison of these whirl test results with free flight measurements show very good compliance with the power and thrust values of one AREA rotor in flettner configuration on the AREA drone.

NOMENCLATURE

ACT	Actuator
AI	Analogue Input
AKD	Programmable Actuator Servo Drive
AREA	Autonomous Rotorcraft for Extreme Altitudes
CAD	Computer-Aided Design
CPL	Telemetry Coupler
cRIO	CompactRIO Controller
CU	Drive Coupling Unit
DAQ	Data Acquisition
EMA	Experimental Modal Analysis
ENC	Telemetry Encoder
ENG	Engine
FEM	Finite Element Method
FS	Full Scale
FU	Frequency Inverter
HMI	Human-Machine Interface
HS	Hall Sensor
LC	Load Cell
MAC	Modal Assurance Criterion
MERIT	Munich Experimental Rotor Investigation Testbed
MSL	Mean Sea Level
PCMM	Programmable Controller Multi-Axis Master
PS	Pressure Sensor
REnc	Rotating Encoder
SG	Strain Gauge
TPU	Telemetry Processing Unit
UL	Ultimate Load
WS	Workstation

$F_{i,j,k}$	i-th component of j-th load cell for load in k-direction
$F_{X,Y,Z}$	rotor hub forces in N
G	balancing quality
h_0	swashplate spherical center height in mm
l	short pitch link length in mm
$M_{x,y}$	rotor hub moments in Nm
M_z	rotor torque in Nm
r	radius of non-rotating pitch link attachment in mm
R_{AREA}	AREA rotor radius in m
R_{MERIT}	MERIT rotor radius in m
R	radius of rotating pitch link attachment in mm
s	pitch horn attachment offset from pitch axis in mm
t	time in s
v_{tip}	blade tip speed in $\frac{m}{s}$
$x_{1,2,3}$	actuator rod positions in mm
α, β	swashplate tilt angles in $^\circ$
Ω	rotor speed in rpm
Ψ	azimuth in $^\circ$
Ψ_0	azimuth of pitch link position in $^\circ$
ρ	density in $\frac{kg}{m^3}$
σ	rotor solidity
θ_0	collective pitch angle in $^\circ$

* Research Associate, v.heuschneider@tum.de
† Research Associate, flo.berghammer@tum.de
‡ Research Associate, tobias.pflumm@tum.de
§ Professor and Department Head, hajek@tum.de

Copyright Statement
The authors confirm that they, and/or their company or organization, hold copyright on all of the original material included in this paper. The authors also confirm that they have obtained permission, from the copyright holder of any third party material included in this paper, to publish it as part of their paper. The authors confirm that they give permission, or have obtained permission from the copyright holder of this paper, for the publication and distribution of this paper and recorded presentations as part of the ERF proceedings or as individual offprints from the proceedings and for inclusion in a freely accessible web-based repository.

This work is licensed under the Creative Commons Attribution International License (CC BY). Copyright ©2021 by author(s).

1. INTRODUCTION

The Munich Experimental Rotor Investigation Testbed (MERIT) is a Mach scaled 85kW rotor test stand. It is designed and built at the Institute of Helicopter Technology, Technical University of Munich, to be used for hover measurements and forward flight tests in TUM´s wind tunnel A at the Institute of Aerodynamics and Fluid Dynamics. The driving design factor for MERIT was the capability of investigating dynamic stall on helicopter rotor blades in high cyclic pitch settings as well as forward flight conditions. Moreover, it serves as a testing platform for fixed pitch propellers and various rotor blade geometries with a radius of up to two meters and a rotational speed up to 3000rpm. Its configuration and robust design allow for experiments outside the standard helicopter rotor envelope.

2. TEST RIG DEVELOPMENT

2.1. Main design targets and specifications

The main design targets of MERIT are summarized in the following points:

1. Dynamic stall capability with Mach scaling
2. Applicability in TUM´s wind tunnel A, Institute of Aerodynamics and Fluid Dynamics
3. Hingeless rotor
4. Loss-free load paths and play-free component interfaces
5. Low eigenfrequencies of the rotor carrying structure
6. Pitch control accuracy: 0.1 °

Points one and two are the basic requirements for the test rig. It should be capable of fundamental dynamic stall research under forward flight conditions. For this purpose, MERIT can be used in TUM´s wind tunnel. Since the wind tunnel's test section width of 2.40m does not allow the use of a geometrically scaled rotor, a Mach scaling of the rotor to a tip speed of $220\frac{m}{s}$ is needed in order to take compressibility effects into account. These basic specifications imply rotor position and size of the test rig.

Points three to five concern the mechanical components' rigidity and eigenmodes. The blade attachment is chosen to be hingeless to avoid an interference of the blade´s pitching movement with flapping or lagging. This allows a the separate analysis of the rotation influence on dynamic stall compared to a pitching airfoil in the wind tunnel. For the very same reason the rotor blade is designed to have a very stiff, monolithic blade attachment section. Play-free component interfaces guarantee a linear load-deformation relation, which simplifies measuring dynamic loads. The stiff component design ensures a reliable rotor load measurement in the stationary frame without dissipation losses. To control dynamic load interactions between the rotor and the basic frame structure, the eigenfrequencies for the basic frame structure should be below the nominal rotor speed (40 to 50 Hz).

The pitch control and measurement accuracy specifications for dynamic stall analyses are set to be lower than 0.1 °.

Structural mass, geometry of the carrying steel frame, blade attachmend type and blade geometry mainly result from the above shown specifications and are considered into more detail in the following.

2.2. Steel frame structure and drive train

The mechanical test rig structure consists of four different welded steel frames: the wind tunnel adaptor welded on clamping pads, the middle frame bolted to the wind tunnel adaptor, the engine cradle bolted to the middle frame, and the bearing frame connected to the middle frame by four three-component load cells [1].

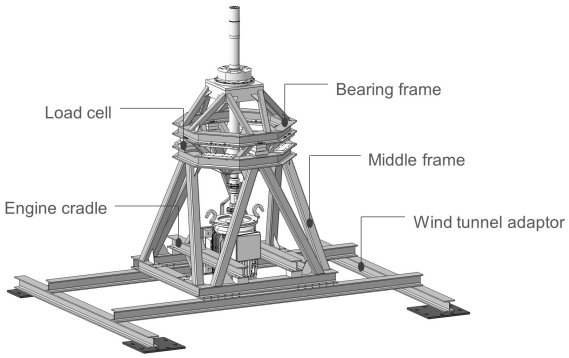

Fig. 1: Steel frame structure with drive train

The bearing frame contains bearings and rotor shaft and serves as fundament for the attachment of actuators, swashplate, pitch links, and the rotor itself. A torsion stiff, bending flexible double gimbal coupling by *KTR Systems GmbH* directly transfers the motor torque to the rotor shaft without gearbox, thus satisfying minimum space and constant speed requirements. The coupling allows for small radial, axial and angular displacements (3.7mm, 2.0mm, 1.0°) and contains a rotor speed and torque measurement unit. The four three-component strain gauge load cells $K3D120 \pm 2kN/VA$, *ME-Meßsysteme GmbH*, measure the rotor forces and moments. The upper frame's pyramidal shape provides high rigidity and a load path with minimal dissipation losses. The 85kW permanent magnet synchronous motor, *3000 LSRPM200L1 85kW V6 400V*, *EMERSON Industrial Automation*, with 3000rpm maximum speed, 270Nm nominal torque, and an incremental encoder with 1024 pulses, is side-mounted to the engine cradle attached to the middle frame [2]. The rotor speed can be controlled through the workstation or an independent HMI

This work is licensed under the Creative Commons Attribution International License (CC BY). Copyright ©2021 by author(s).

touch panel and handwheel directly connected to the frequency inverter´s control unit. This architecture provides minimal failure proneness and maximum data speed.

2.3. MERIT rotor

For application in TUM´s wind tunnel A, the main rotor disk shall be located in the middle of the wind tunnel working section (2.40m wide, 1.80m high). With a height of 1.70m of the basement ground to the wind tunnel test section ground, the rotor height is 2.60m from the ground. The hingeless main rotor provides space for the attachment of four, two or one rotor blade. This should prevent an overlapping of blade flap and lead-lag motion with the blade´s pitch movement during dynamic stall and thus ensure the sole investigation of the rotational speed influence on the phenomenon. Fig. 2 shows the rotor head with two blade attachments. A clamping set provides the frictionally engaged connection between the rotor head and the shaft. Each blade holder is mounted to a bushing by a pair of needle bearings. This bushing is radially screwed to the rotor head. A torsion soft metal sheet stack provides the centrifugal force load suspension and serves as a torsion-tension strap. One stack consists of 34 cold-rolled feather steel (1.4310) sheets, each 0.3mm thick. In contrast to axial bearings this sheet stack has a very high loading capacity as shown in the *Component testing* section. This functionality is especially advantageous at high rotor speeds, since centrifugal forces of up to 60kN at rotational speeds up to 3000rpm are expected. The blade holders carry a magnet ring *PMIR7-20-90-M-50* by *ASM Automation Sensorik Messtechnik GmbH* to measure the blade pitch angle. The respective hall sensor *PMIS4-20-40-240KHZ-TTL-Z1-2M-S*, *ASM Automation Sensorik Messtechnik GmbH*, is attached to the rotor head, right below the magnet ring with a gap of approximately 0.1mm.

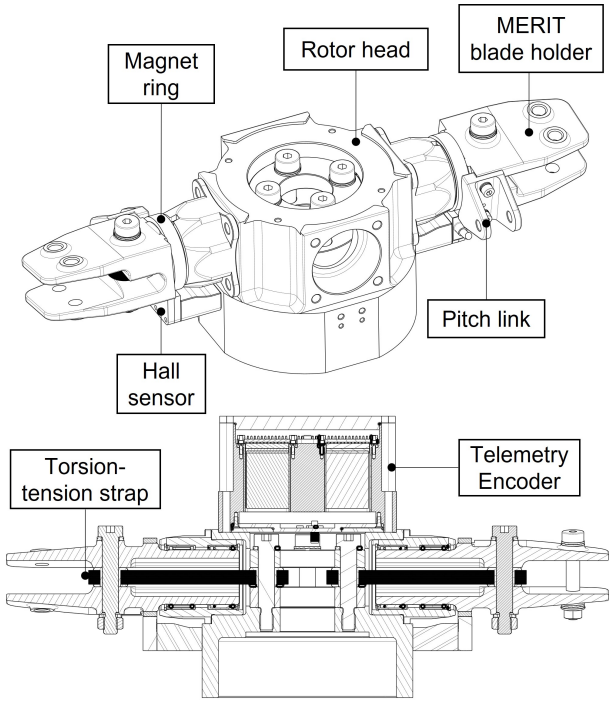

Fig. 2: Rotor head with two blade attachments in isometric and sectional view without and with telemetry encoder on top

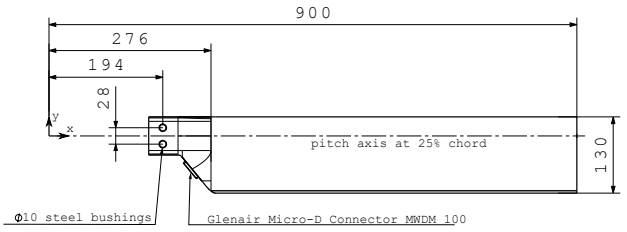

Fig. 3: MERIT rotor blade

MERIT´s first set of rotor blades was specifically designed for dynamic stall. It is kept very simple in its geometric design to easily compare rotating measurements with non-rotating pitching airfoil wind tunnel measurements. It has a rectangular planform with zero twist and no taper, a 130mm chord, and the symmetric NACA0012 airfoil geometry including tap. Applicability in TUM's wind tunnel restricted the rotor diameter to 1.80m to prevent interaction of wind tunnel shear layers with the dynamic stall vortex. The rotor blade is a full carbon structure with a C-spar as well as a monolithic blade attachment and blade tip section for the integration of blade bushings and a balance cell.

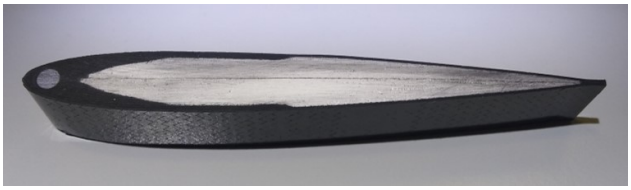

Fig. 4: MERIT rotor blade section

The titanium balance cell integrated into the blade tip at the quarter cord provides space for up to 7.7g tungsten. The holes for the balance cell and the attachment bushings were drilled with specifically designed positioning devices to provide the specified position accuracy of minimum 0.01mm. Balance cell and bushings were glued into the holes using small fitting surfaces, which allow for an accurate positioning as well as the right adhesive gap size. The rotor blade is built in a two-stage manufacturing process with carbon fibre prepregs. In this way, pressure or strain sensors can easily be positioned and integrated into the cured skin layers of each half shell, before inserting the remaining spar layers, nose lead and foam core halfs.

An embededd Glenair connector (*GLENAIR Micro-D MWDM 100*) serves as a robust interface and can be equipped with either 100 electical contacts or 8 fiber optical termini. A layer of the shielding fabric *Aaronia-Shield*

This work is licensed under the Creative Commons Attribution International License (CC BY). Copyright ©2021 by author(s).

with up to 50dB damping at 1GHz can be integrated into the skin layers of the blade and shields the sensitive sensor cables from noise due to electromagnetic waves. The first three serial blades contain a substitute connector dummy and no instrumentation inside. A more detailed description of the blade design and manufacturing process can be found in [3].

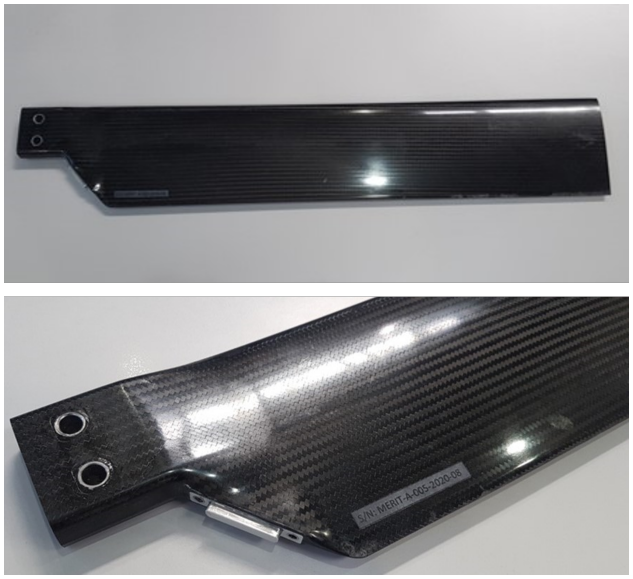

Fig. 5: MERIT rotor blade

Fig. 6 shows the setup for the balancing of the two MERIT blades *S/N: MERIT-A-006-2021-03* and *S/N: MERIT-A-008-2021-04* (A: revision, 008: sequential number, 2021-04: manufacturing year and month). Their masses before balancing were 833.3g and 839.5g. Aiming at a balance quality of G2.5, according to DIN ISO 1940 [4], which implies a permissible imbalance of 20gmm at 2300rpm regarding two rotor blades of 1kg maximum weight each, we used a three-component force/moment cell to measure the resulting static imbalance [5] [6]. Due to the crosstalk of the vertical load onto the perpendicular moments (0.0008 Nm/N), a lathed calibrating steel plate was used to zero the crosstalk moments in the operating point of the two blades' total weight. With an additional mass of 2.8g on *S/N: MERIT-A-006-2021-07* a remaining static imbalance of 30.42 gmm was achieved.

The stiffness properties of the blade were determined with static deformation measurements (Fig. 7) using Digital Image Correlation (DIC) to measure the strain and displacement field. Torsion, bending moments, tensile and shear forces were applied at the blade tip and measured by a six-component load cell at the blade attachment [7]. The results of the sectional stiffness properties derivation are presented in [3] and [8].

2.4. Swashplate actuation

The swashplate is desined for the actuation of four, two or one rotor blade with counterweight. It contains a spherical brass bearing sliding vertically on the rotor shaft and thus granting translational and rotational degrees of freedom for collective and cyclic pitch control, see Fig. 8.

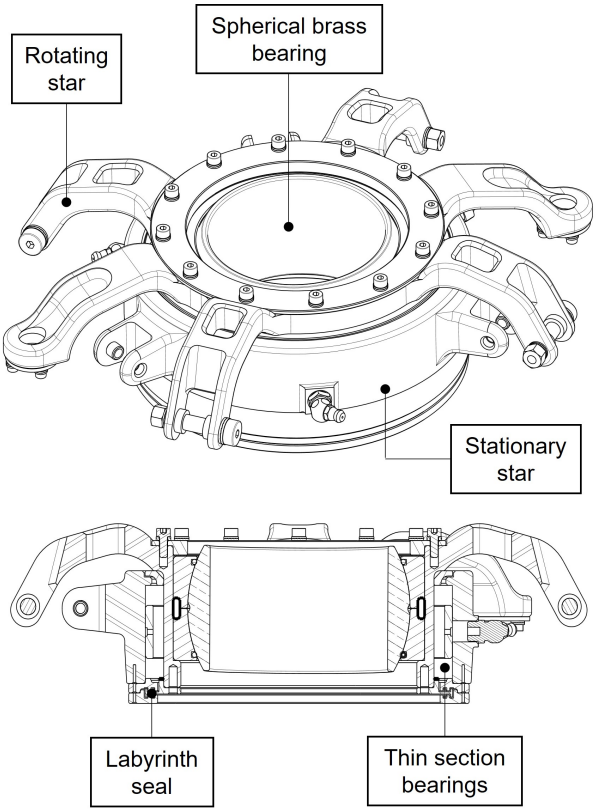

Fig. 8: Swashplate with spherical bearing

It is actuated by three linear, electromechanical roller screw actuators with integrated motors *DA67-22-75*, *Diakont*, mounted with a 120° angular offset to each other. The roller screw mechanism provides more cumulative contact surface and thus very high accuracy and rigidity. Detailed actuator parameters are listed in Tab. 1. The combination of actuators and swashplate kinematics results in a pitch angle control accuracy of 0.025°.

Entity	Value	Unit
Max. continuous force	2670	N
Peak force	5560	N
Max. dynamic load	25270	N
Max. speed	208	mm/s
Lead accuracy	0.025/0.3	mm/m
Nominal backlash	0.1	mm

Table 1: DA67-22-75 linear roller screw actuator parameters, [9]

Three programmable actuator servo drives (*AKD-P00606-NBCC*) from *KOLLMORGEN Europe GmbH* con-

This work is licensed under the Creative Commons Attribution International License (CC BY). Copyright ©2021 by author(s).

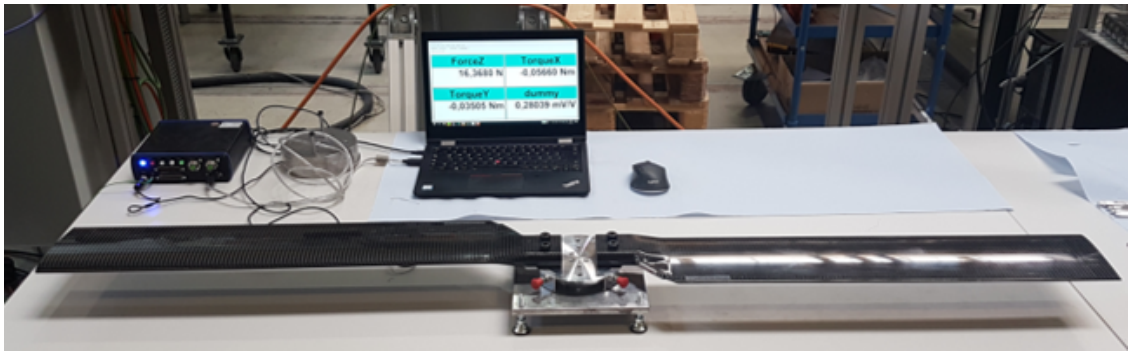

Fig. 6: MERIT rotor blade balancing

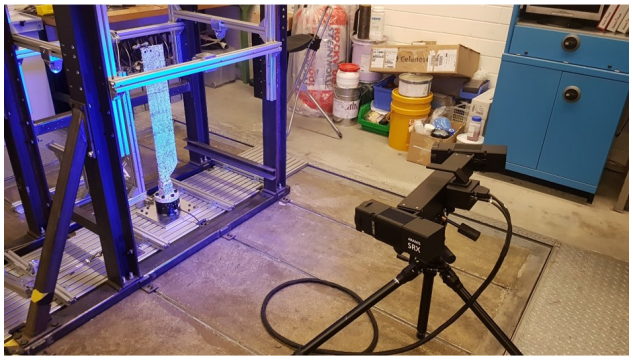

Fig. 7: Static deformation measurements using DIC

trol the actuators each. These are integrated into an Ethercat cycle controlled by a Programmable Controller Multi-Axis Master (*AKC-PCM-M1-120*, short *PCMM*), *KOLL-MORGEN Europe GmbH*. This configuration allows for the synchronous movement of the actuators to tilt the swashplate around its predefined longitudinal and lateral cyclic control axes and to vertically move the swashplate as a whole. Analogous to the rotor speed control, the actuator control can be accessed either through the workstation or a fully independent HMI touch panel directly communicating with the *PCMM*.

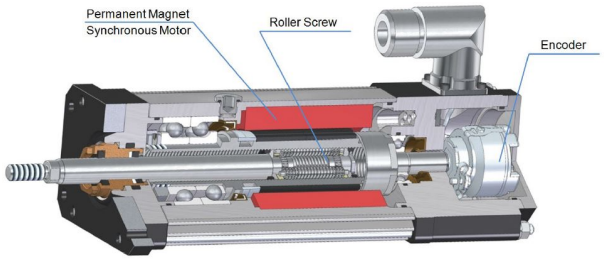

Fig. 9: Electromechanical roller screw actuator *DA67-22-75*, *Diakont*, [9]

The underlying equations for the relation between the actuator rod positions x_1, x_2, x_3, the swashplate's tilt angles and vertical position α, β, h_0, and the blade control angles $\Theta_0, \Theta_S, \Theta_C$ are given as

$$(1) \quad \begin{bmatrix} \frac{1}{3} & \frac{1}{3} & -\frac{1}{3} \\ 0 & \frac{1}{2r\cos 30^\circ} & -\frac{1}{2r\cos 30^\circ} \\ \frac{2}{3r} & -\frac{1}{3r} & -\frac{1}{3r} \end{bmatrix} \begin{bmatrix} x_3 \\ x_1 \\ x_2 \end{bmatrix} = \begin{bmatrix} h_0 - l \\ \alpha \\ \beta \end{bmatrix}$$

$$(2) \quad \begin{bmatrix} -\frac{1}{s} & 0 & 0 \\ 0 & -\frac{R}{s} & 0 \\ 0 & 0 & -\frac{R}{s} \end{bmatrix} R \begin{bmatrix} h_0 - l \\ \alpha \\ \beta \end{bmatrix} = \begin{bmatrix} \Theta_0 \\ \Theta_S \\ \Theta_C \end{bmatrix}$$

with

$$(3) \quad R = \begin{bmatrix} 1 & 0 & 0 \\ 0 & \cos\Psi_0 & \sin\Psi_0 \\ 0 & -\sin\Psi_0 & \cos\Psi_0 \end{bmatrix}$$

$$(4) \quad \Theta(t) = \Theta_0 + \Theta_C \cos\Omega t + \Theta_S \sin\Omega t$$

l, r, R, s, Ψ_0 are constant parameters resulting from the mechanical components' geometry.

2.5. Instrumentation and data acquisition

The instrumentation in the stationary frame consists of four three-component load cells between the bearing frame and the middle frame, measuring the global rotor forces and moments, and the drive coupling unit, measuring torque and rotor speed.

This analog sensor data is acquired and processed using the *National Instruments* real-time controller *CompactRIO*. The *CompactRIO* chassis uses an onboard processor and a Linux based operating system to digitalize and synchronize incoming data, and provides space for up to eight different measurement cards. We use four *NI9237* Modules (4 AI, 24Bit, 50kS/s/ch) for the force load cell signals, two *NI9401* Modules (8 DIO, 5V TTL, 100ns) for the rotating encoder and coupling TTL signals, and one *NI9205* Module (16 AI Differential, 16Bit, 250kS/s) for the analog coupling signals (speed and torque) [10] [11] [12].

The rotating system uses a 32-channel, inductive telemetry system with a 20kS/s sampling rate by *MANNER*

This work is licensed under the Creative Commons Attribution International License (CC BY). Copyright ©2021 by author(s).

Sensortelemetrie GmbH. The respective encoder is placed on top of the rotor head, and amplifies and digitalizes analog sensor data in the rotating frame. It allows short analog sensor cabling and hereby small susceptibility to electromagnetic noise. The analog data is lead down to the power/data coupler within the center of the rotor shaft. The contact-free, inductive data transmission technology is space-saving and wear-free in contrast to commonly used slip rings. A telemetry processing unit assesses the digital data and provides the power and voltage needed for the sensors. Any kind of sensor data based on a Wheatstone bridge can be processed with the telemetry system, such as strain gauges, pressure sensors, etc.

Hall sensor and magnetic ring		
Manufacturer	*ASM*	
Type name sensor	*PMIS4-20-40*	
Type name ring	*PMIR7-20-90*	
Max. impulse frequency	240	kHz
Pulses	3600	1/rev
Accuracy	0.025	°
3-Component Load Cell		
Manufacturer	*ME*	
Type name	*K3D120*	
Nominal force x,y,z	$\pm$ 2000	N
Max. load	150	%FS
Accuracy	0.5	%
Crosstalk	1	%
Nominal deformation	0.06	mm
Rotating Encoder		
Manufacturer	*Globalencoder*	
Type name	*IH150*	
Pulses	1024	1/rev
Azimuthal Resolution	0.088	°
Max. speed	4000	rpm
Coupling Unit		
Manufacturer	*KTR*	
Type name	*DATAFLEX32*	
Max. torque	500	Nm
Accuracy	0.1	%
Pulses	720	1/rev
Azimuthal Resolution	0.125	°
Max. speed	7500	rpm
Inductive Telemetry		
Manufacturer	*MANNER*	
Number of channels	32	
Sampling rate	20	kS/s
Resolution	16	bit
CompactRIO		
Manufacturer	*NI*	
Type name	*cRIO 9047*	
Timing resolution	12.5	ns
Sample clock frequency max.	10	MHz
Internal Storage SSD & RAM	4	GB

Table 2: Sensor and DAQ parameters [13] [14] [15] [16] [17]

Each blade attachment carries a magnetized ring with the respective hall sensor underneath to measure the blade pitch angle. Using high and low slopes of both TTL signals A and B for each sensor achieves an angular measurement accuracy of 0.025°, which is four times the accuracy given in the sensor´s data sheet.

In addition to the rotating encoder in the coupling measurement unit, a second one is mounted to the rotor shaft to measure the shaft speed more accurately. It is used by the telemetry processing unit to trigger the data sampling once per revolution at azimuthal angle $\Psi = 0^\circ$. The same encoder signal is acquired by the *CompactRIO* controller for synchronization purposes. Table 2 summarizes the most significant sensor and DAQ equipment information. Live data processing and viewing of both stationary and rotating sensor data is done with *Labview*.

Data synchronization between the rotating and stationary data is achieved by using the $\Psi = 0^\circ$ position of the rotating encoder to trigger the analog data acquisition of the *CompactRIO*. The rotational speed and angular position signals are processed and saved with both the Telemetry Processing Unit (TPU) and the *CompactRIO*. Rotating and stationary data can be synchronized in the postprocessing by using the rotating encoder signal to eliminate possible time shift. The trigger accuracy itself depends on two main factors: the sampling rate and the trigger´s minimal impuls width. With a sampling rate of 20kS/s and a minimum impulse width of $3 \cdot 10^{-5} s$, the latency lies at maximum $80 \mu s$ [18].

Another time delay concerning synchronization should be mentioned, which is the delay due to the conversion time within each module of the *CompactRIO*. This time lag varies from $1.6 ms$ to $100 ns$ depending on the module. Each module's delay can be regarded constant and added to the respective signal timing in *Labview*.

An overview over the equipment used for actuator and motor control, sensing, and data acquisition as well as processing can be seen in Fig. 10. The measurement system´s architecture with the flow of information is shown in Fig. 11.

2.6. Load cell calibration

As stated above, the four load cells measuring the global rotor forces and moments are mounted between the upper bearing frame and the middle frame, see Fig. 12. Two opposing load cell centers have a distance of 891mm to each other. The load cells are aligned with register pins on surfaces of both frames, which are milled in one clamping operation each to provide a positioning accuracy of at least 0.01mm. Likewise, the fits for the shaft bearings were milled together with the load cell attachments in one clamping operation to guarantee perpendicularity between the rotor shaft and the load cell contact faces. The set of load cells are calibrated by applying an axial and transverse force in an interval of 45° azimuthal angle at the rotor head. The force is applied using steel ropes, deflection pulleys and

This work is licensed under the Creative Commons Attribution International License (CC BY). Copyright ©2021 by author(s).

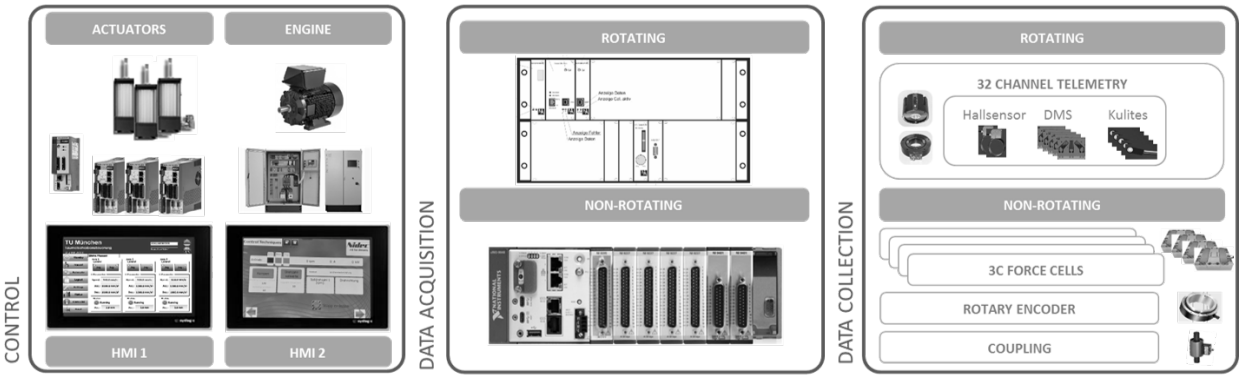

Fig. 10: Control, DAQ and sensing equipment

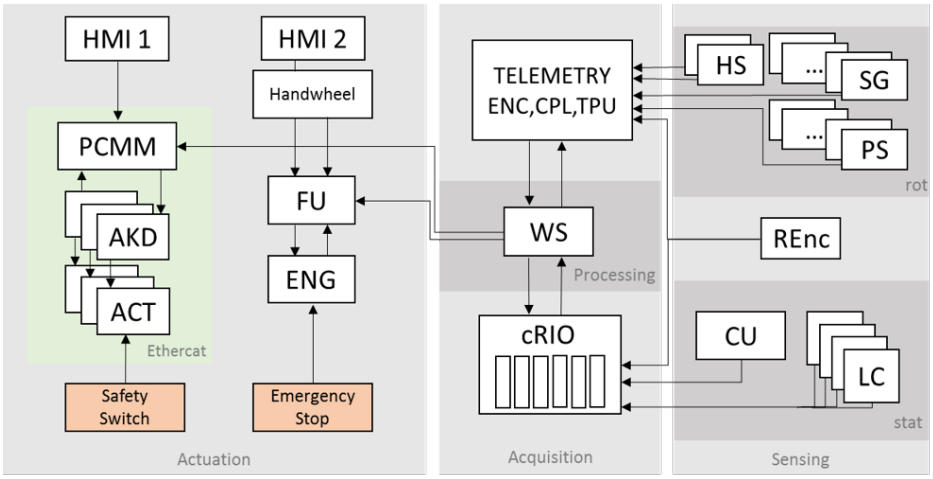

Fig. 11: MERIT´s actuation and measurement system architecture

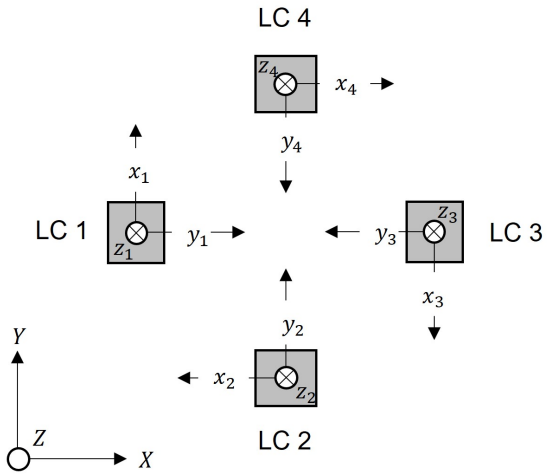

Fig. 12: Load cell setup in a top view

weights implying a calibration load F_{cal} up to 378N. The direction of force application is aligned with a self-levelling laser. Fig. 13 shows the load results at the example of axial load application in global $-Z$ direction. Each load cell´s force component and the resulting sum in dependence of the calculated calibration force are given. The manufacturer's calibration information concerning crosstalk between the axes of each load cell are taken into account.

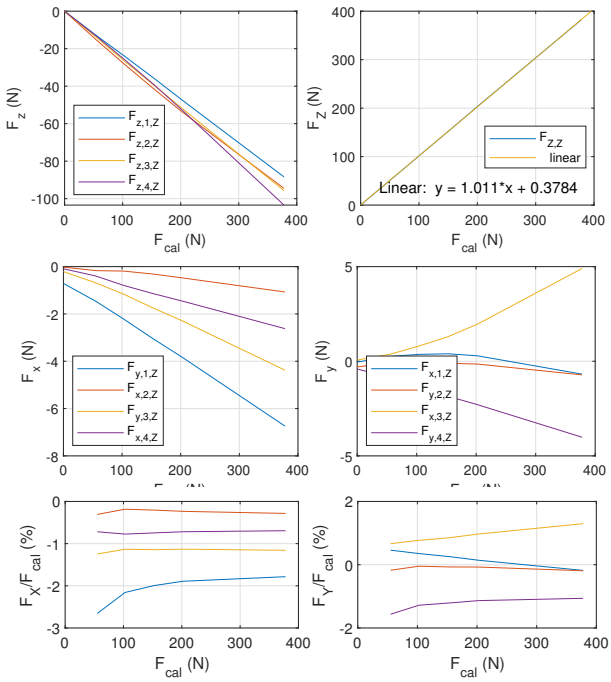

Fig. 13: Load cell calibration force results for axial load

This work is licensed under the Creative Commons Attribution International License (CC BY). Copyright ©2021 by author(s).

The z-components of all load cells $F_{z,1,Z}, F_{z,2,Z}, F_{z,3,Z}, F_{z,4,Z}$ show that the load is not equally shared, whereas the sum of the z-components shows a very good linear behaviour, that can be fitted with a linear with the slope 1.011 and a norm of residuals of 0.779. The x- and y-components show a load under 2% of an applied load $F_{cal} \geq 200N$. The force and moment graphs for transversal loads in $+X, -X, +Y, -Y$ direction are given in the appendix.

The following transformation matrix A for the global forces $F_{x,y,z}$ and moments $M_{x,y}$ could be derived from all calibration measurements [18]:

$$A = \begin{bmatrix} 1.0108 & 0.0088 & 0.0089 & -0.0064 & 0.0069 \\ 0.0011 & 0.9907 & -0.0067 & 0.0047 & 0.0008 \\ 0.0040 & 0.0037 & 1.0107 & -0.0027 & 0.0029 \\ 0.0122 & -0.0088 & -0.0115 & 1.0065 & 0.0089 \\ 0.0129 & 0.0133 & 0.0087 & -0.0097 & 1.0094 \end{bmatrix}$$

The primary diagonal entries show a deviation of max. 1.08% from 1.0. The maximum minor diagonal element being 1.33% shows that the overall crosstalk is small.

2.7. Component testing

2.7.1. Modal analysis on steel frame

For a safe initial operation, we performed an Experimental Modal Analysis (EMA) on the steel frame structure including rotor shaft and bearings to identify natural frequencies, mode shapes and damping characteristics of critical eigenmodes below 50 Hz, which is the maximum nominal rotor speed. Unsurprisingly, eigenmodes below 50Hz mainly result from the wind tunnel adaptor´s long beam motions and the load cell passage between bearing and middle frame [19]. Table 3 shows the eigenfrequencies identified with the EMA and the FEM calculations. The frequencies were matched using the Modal Assurance Criterion (MAC) [20]. More detailed information on the experimental setup, the mode shapes and damping ratios or the FE model can be found in [19].

Mode	1	2	3	4	5	6
EMA (Hz)	7.45	13.34	15.81	19.48	31.88	46.97
FEM (Hz)	6.00	11.58	13.31	23.20	44.21	54.98
MAC (-)	0.88	0.96	0.86	0.87	0.89	0.71

Table 3: EMA and FEM frequency, and MAC table for eigenmode one to six of the steel frame and drive train [20], [19]

2.7.2. Tensile strength tests

To further ensure operational safety, tensile strength tests were carried out with relevant components representing the critical spots of the test rig. Considering structures with a failure resulting in imbalance, major damage scenarios and emergency stop of the test procedure led to the three most crucial failure modes of the test rig in operation emerging from the rotating system, Tab. 4.

Failure Mode	Expected UL (kN)
Balance cell unbonding	1.33
Blade-off	80.69
Metal sheet stack rupture	105.20

Table 4: Relevant failure modes and expected ultimate loads

Fig. 14 shows the results of the tensile strength tests of the three critical components: the blade attachment section, the balance cell, and the metal sheet stack.

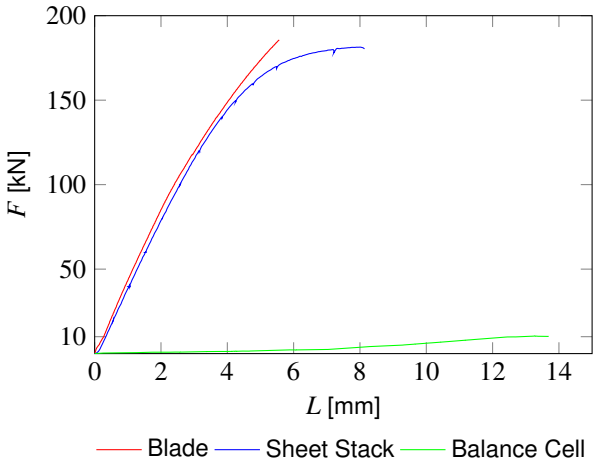

Fig. 14: Results from tensile strength tests

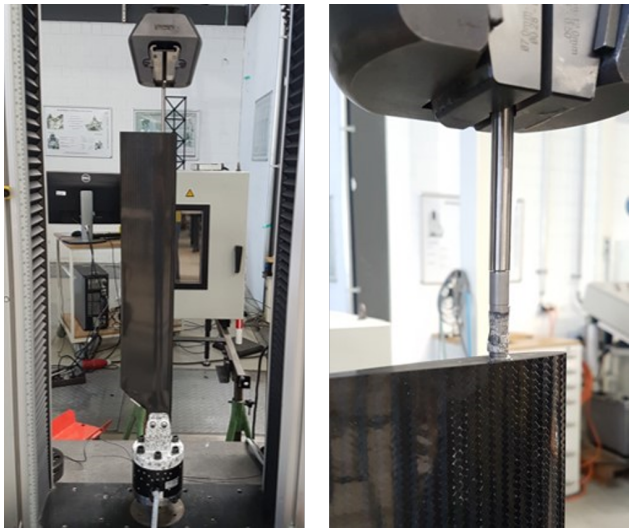

Fig. 15: Tensile strength test of the blade tip balance cell

Fig. 15 shows the setup for static testing at the Laboratory for Product Development and Lightweight Design,

This work is licensed under the Creative Commons Attribution International License (CC BY). Copyright ©2021 by author(s).

TUM. The balance cell was glued into the monolithic section of the blade tip using *3M SCOTCH-WELD EC-9323 B/A* two component adhesive. A threaded pin adaptor connects the balance cell to the clamping device.

To enable redundant force measurement and ensuring alignment of the load path in radial direction of the blade, a six-component load cell was installed in addition to the integrated device of the test stand [7]. As shown in Fig. 14, the expected ultimate load [21] for unbonding of the balance cell could be exceeded and cohesive failure was observed.

Concerning blade-off scenario, the MERIT rotor blade had to be modified for tensile strength testing. To provide a correct load application to the blade root section without provoking a failure within the bolts section of the adapter for the tensile testing machine, additional layups were laminated onto the shortened blades surface. Interlaminar shear failure of the C-spar could be observed at a load of more than twice the expected ultimate load (see Fig. 17 and Fig. 14) during static tensile testing at the Institute of Materials Science and Mechanics of Materials, TUM. A stochastic speckle pattern was applied to measure the strain field again with DIC.

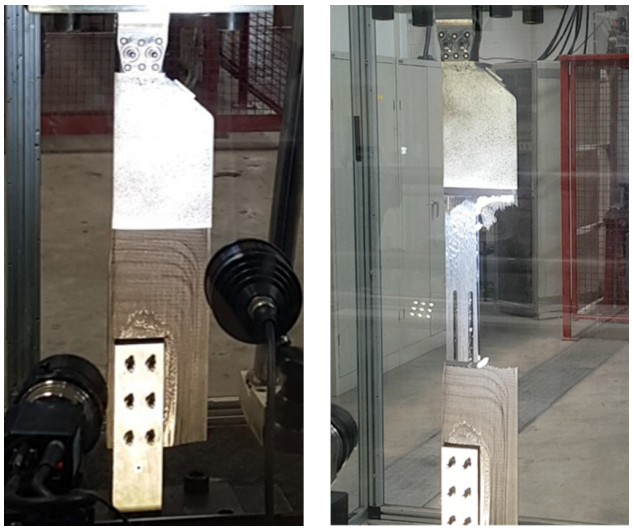

Fig. 16: Centrifugal force tensile strength test of the rotor blade

Experiencing the highest centrifugal forces, the metal sheet stack acts as the structure's torsion-tension strap and hence needs to be investigated to ensure fail safe operation. As seen in Fig. 2, the metal sheet stack carries centrifugal forces from the blade attachment's weight as well as the weight of the blade and itself during operation.

Static tensile tests did not lead to failure of the sheet stack itself, but rather resulted in ductile shear failure of the 12mm diameter bolts used for the attachment as seen in Fig. 17. The sheet stack's ultimate load is almost the same as the one of the blade itself, but shows a lot more ductile behaviour, see Fig. 14.

Fig. 17: Centrifugal force tensile strength test of the metal stack

3. INITIAL HOVER TEST RESULTS

The initial operation of MERIT was performed with the two left-rotating blades of the AREA drone, which uses two main rotors in a flettner configuration [22], [23]. The AREA blade is a full-carbon blade with linear taper of 0.6 and a linear twist of -10° and is specifically designed for operations in high altitudes [24]. The rotor has a radius of 1.669m when mounted on the AREA drone, 1.723m when mounted on the MERIT test rig. The respective rotor solidities are given in Tab. 5. Figure 19 shows the blade´s dimensions.

AREA	AREA drone	MERIT test rig
Rotor radius R	1.669m	1.723m
Rotor solidity σ	0.031	0.0291

Table 5: AREA rotor radius on the flettner drone vs. on MERIT [22]

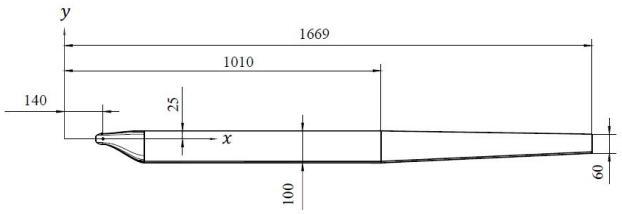

Fig. 19: AREA rotor blade dimensions in mm when mounted on the AREA drone [22]

To mount the AREA rotor blades on the MERIT rotor head, the blade holder had to be modified at the side of the blade attachment, whereas the attachment parts on the rotor head side (metal sheet stack, pitch bearing shaft, magnet ring, pitch link) were left without adjustments. The two bolts are replaced with one 6 mm diameter bolt, which serves as a lead-lag hinge. We used an additional hard-anodized, aluminum (EN AW 7075) blade casting element between the blade holder and the rotor blade for two main reasons. On the one hand it preserves the blade's surface

This work is licensed under the Creative Commons Attribution International License (CC BY). Copyright ©2021 by author(s).

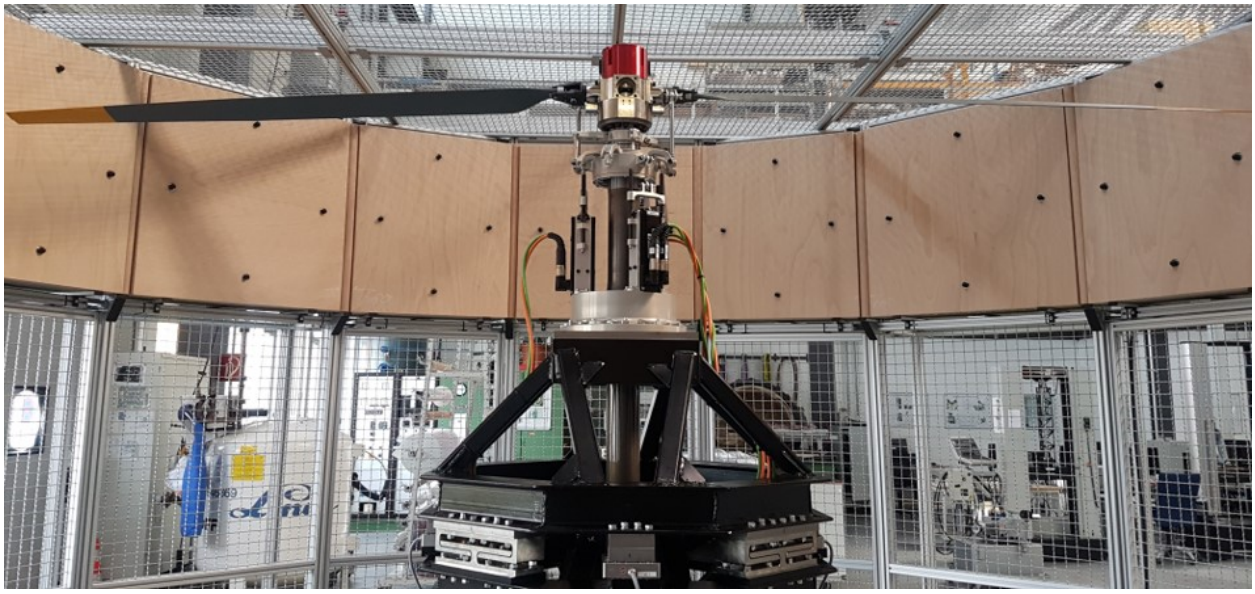

Fig. 18: Left rotating AREA rotor on the MERIT test rig

quality and protects it against abrasion, on the other hand it provides a mechanical lead-lag limitation, since the blade casting has two symmetric stop collars, that will get in contact with one of two lead-lag limitation bolts, if an abrupt rotor deceleration or acceleration occurs. This should prevent damage on the rotor blade, when a hard stop is necessary.

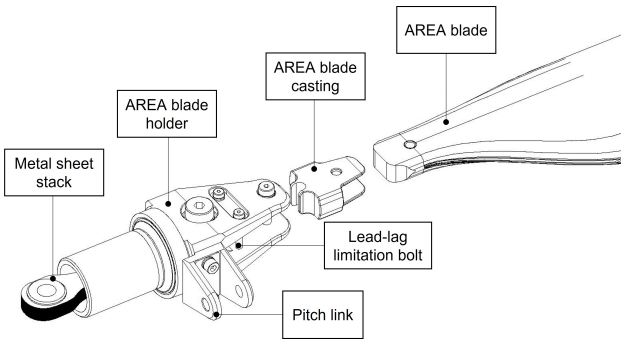

Fig. 20: AREA rotor blade holder on MERIT rotor head

The AREA rotor performance in flettner configuration on the drone was measured for hover tip speeds up to 140m/s and five different total weights, which imply hover thrusts between $182N$ and $282N$, see Figure 22 [22]. For MERIT´s power and thrust measurement verification, the AREA rotor´s polar measurements were performed on MERIT choosing the rotational speeds of $\Omega = 550, 600, ..., 800\ rpm$, and thus the tip speeds $v_{tip} = 99.2, 108.3, 117.3, 126.3, 135.3, 144.3\ \frac{m}{s}$, which were chosen to at least cover the rotor tip speeds 100 to $140\ \frac{m}{s}$ on the drone. The collective pitch angles were set to $\Theta_0 = 0°, 1°, ..., 12°$.

Figure 21 shows rotor thrust and power needed at the above defined collective pitch angles and rotor speeds.

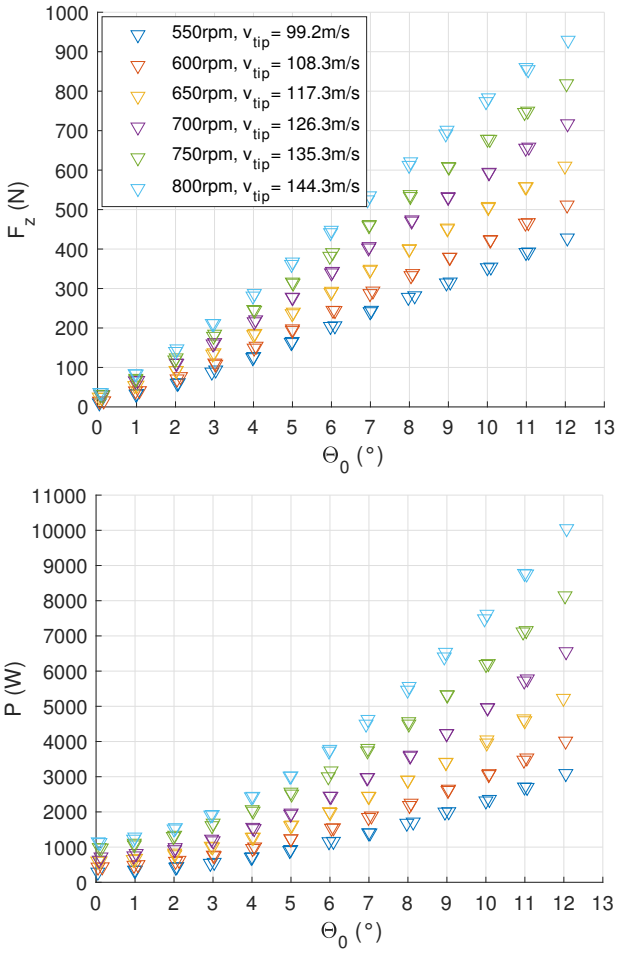

Fig. 21: AREA rotor thrust F_z and power P over Θ_0

It should be noted here that the power shown here is approximately the power used for the rotation of the rotor

This work is licensed under the Creative Commons Attribution International License (CC BY). Copyright ©2021 by author(s).

blades. The power for driving the shaft, rotor head, and blade attachments including the dissipation power within the bearings is subtracted. This power lies between $514\ W$ for $550\ rpm$ and $922\ W$ for $800\ rpm$.

A comparison of thrust values for single operation points defined by collective pitch and tip speed shows good agreement of the AREA-on-MERIT measurement data with the CAMRAD II simulation and AREA-on-drone measurements from [22] within the a speed range of 100 to $140\frac{m}{s}$ and a thrust range of 182 to $282N$ per rotor, see Fig. 22.

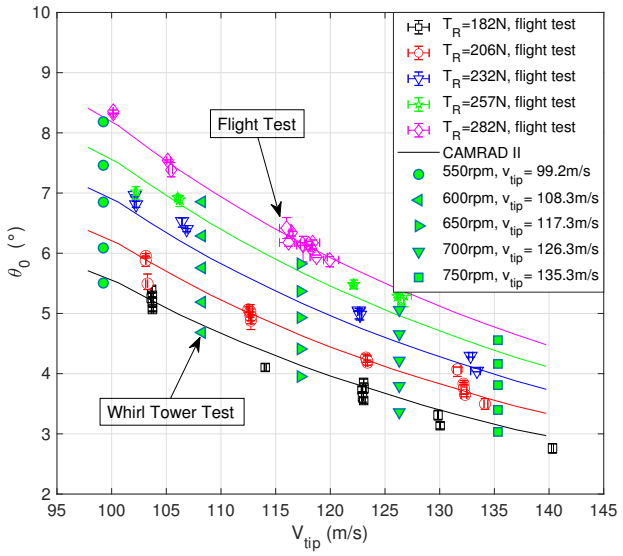

Fig. 22: Comparison of AREA flight test data (intermeshing rotors), CAMRAD calculations, and whirl tower data (single rotor) for five different rotor thrusts; flight test at 500m MSL [22]

To get the shown values the $F_z(\Theta_0)$ data was interpolated at the five discrete, single-rotor thrust values, that had to operate on one interacting AREA drone rotor in order to carry five different drone weights in hover at 500m MSL. The results show that the AREA rotor in the whirl tower measurements needs less collective pitch Θ_0 to achieve the same rotor thrusts as the AREA rotor on the drone.

Regarding C_P/σ over C_T/σ for the two rotor configurations (Fig. 23), AREA on drone (free flight test) and AREA on MERIT (whirl tower test), it is obvious that the rotor on the MERIT test rig needs less power than on the drone. There are several reasons that can lead to this effect.

1. The drone measurement results show the power needed for a single AREA rotor interfering with the second rotor in synchropter configuration. Due to the inflow disturbances by the interference with the second rotor, more power is needed to produce the same lift as for the AREA rotor on the test rig.

2. Since the power needed for rotation of all rotor components other than the rotor blades was subtracted, it might lead to slightly fewer power than the power measured on the drone´s rotor shaft directly below the rotor head.

3. The AREA blade tip radius is 54mm higher on the MERIT test rig than on the drone. For the best comparability of both measurements this was compensated by lower rotational speed, thus keeping the blade tip speed almost the same. Nevertheless, the radial speed distribution is not equal in both cases and will result in slightly different thrust and power values.

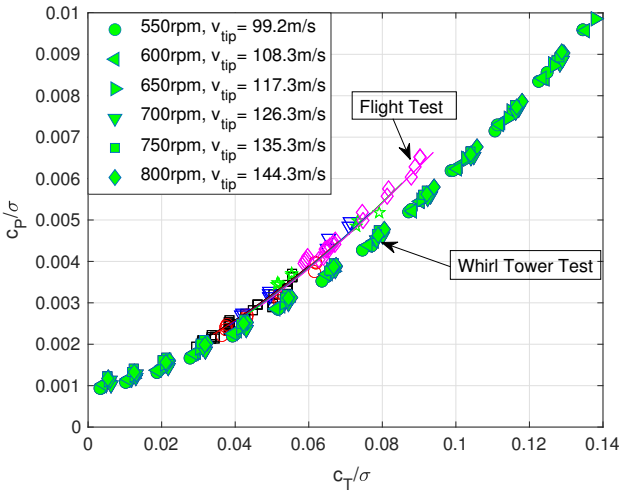

Fig. 23: Comparison of AREA hover polar C_P/σ over C_T/σ from flight test data with whirl tower tests

CONCLUSIONS AND OUTLOOK

This paper portrayed the development and design of the Mach scaled rotor test rig MERIT, including mechanical components development and testing, measurement equipment, and data acquisition architecture. It concludes with first hover thrust and performance test results of the AREA rotor´s polars, which are compared to free flight hover test data. The following conclusions can be drawn from the results shown above:

1. The Institute of Helicopter Technology built a Mach scaled test rig which meets the main design targets. The main eigenfrequencies of the carrying structure are below 50Hz and the required pitch angle accuracy of 0.1 ° could be satisfied with an actual control and measurement accuracy of 0.025 °.

2. The calibration results for the setup with four load cells show a linearity deviation and load measuring accuracy at about 1% and a crosstalk of under 2%.

3. MERIT´s rotating and stationary measurement system is feasible of acquiring, processing and synchronizing currently available data: rotor forces, rotor shaft

This work is licensed under the Creative Commons Attribution International License (CC BY). Copyright ©2021 by author(s).

torque, rotational speeds and blade incidence angle (collective, longitudinal cyclic, lateral cyclic) at a sampling rate of 20kS/s.

4. The hover test results and their comparison to the AREA drone measurements show that the AREA rotor on the whirl tower needs slightly less collective pitch command to achieve the same thrust as one interacting rotor in the flight test.

5. The AREA rotor on MERIT needs less power for the same thrust and tip speed due to a different drive train, blade attachment, rotor diameter and the absence of interference effects with a second rotor.

Further measurements are needed to analyse repeatability, atmospherical effects, and possible interference effects between the tip vortex and the test rig´s containment wall, since the tip spacing thereof is 477mm. The next steps comprise polar measurements for the MERIT rotor with strain gauge instrumentation of the blade root and pitch links.

ACKNOWLEDGMENT

The authors would like to thank the mechanical lab at the Physics Department, TUM, and the Institute of Product Development and Lightweight Design, TUM, for their support to build and assemble MERIT. Moreover, we thank the Institute of Materials Science and Mechanics of Materials including the Material Testing Department for their flexible and supportive cooperation, as well as Benedikt Sosa, B.Sc., who greatly contributed to the data acquisition process during his mid term thesis.

REFERENCES

[1] Sixt, H., “Conceptual Design and Construction of the Main Shaft, Bearing and Steel Frame for a Helicopter Rotor Test Rig,” *Master’s Thesis*, 2017.

[2] Emerson Industrial Automation, *Permanent Magnet Motor 3000 LSRPM200L1 85kW V6 400V Technical Data Sheet*, 2016.

[3] Pflumm, T., Gaugelhofer, L., Heuschneider, V., Berghammer, F., and Hajek, M., “Hybrid Experimental Measurement of Sectional Stiffness Properties of the MERIT Rotor Blade with Digital Image Correlation,” *Proceedings of the 47th European Rotorcraft Forum*, Royal Aeronautical Society, Virtual, September 2021.

[4] Deutsches Institut für Normung (DIN), *Mechanical vibration - Balance quality requirements for rotors in a constant (rigid) state - Part 1: Specification and verification of balance tolerances (ISO 1940-1:2003)*, 2004.

[5] Roth, N., “Konzept und Konstruktion einer Auswuchtvorrichtung für Rotorblätter des experimentellen Rotorprüfstandes MERIT,” *Bachelor´s Thesis*, 2020.

[6] ME Messsysteme GmbH, *K3R70 20N/200mNm, Technical Data Sheet*, 2020.

[7] ME Messsysteme GmbH, *K6D130 5kN/500Nm, Technical Data Sheet*, 2021.

[8] Gaugelhofer, L., “Hybrid Experimental Measurement of Sectional Stiffness Properties of a Composite Rotor Blade with Digital Image Correlation,” *Master´s Thesis*, 2020.

[9] Diakont, *DA Series Electric Roller Screw Actuators with Integrated Motors, Technical Data Sheet*, 2020.

[10] National Instruments, *NI 9237 Technical Data Sheet*, 2015.

[11] National Instruments, *NI 9401 Technical Data Sheet*, 2015.

[12] National Instruments, *NI 9205 Technical Data Sheet*, 2015.

[13] ASM Automation Sensorik Messtechnik GmbH, *posimag® rot, Magnetische Inkrementalencoder, PMIS4, PMIR7, PMIR7N, Technical Data Sheet*, 2021.

[14] ME Messsysteme GmbH, *K3D120 ±2kN/VA Technical Data Sheet*, 2019.

[15] KTR Systems GmbH, *DATAFLEX 32 (DMS) Technical Data Sheet*.

[16] National and Instruments, *CompactRIO Controller cRIO 9047 Technical Data Sheet*, 2015.

[17] MANNER Sensortelemetrie GmbH, *Telemetriesystem Bedienungsanleitung, 32-Kanal, PCM, RMC, RPM, Ethernet*, 2021.

[18] Sosa, B., “Real-Time Sensor Data Acquisition and Synchronization for the Rotor Test Rig MERIT,” *Mid Term Thesis*, 2021.

[19] Heuschneider, V., Berghammer, F., and Hajek, M., “Numerical and Experimental Study on the Modal Characteristics of a Rotor Test Rig,” *Topics in Modal Analysis & Testing, Volume 8*, Springer International Publishing, 2020.

[20] Berghammer, F., “Vibration Behaviour Modelling and Analysis of a Helicopter Rotor Test Rig,” *Master’s Thesis*, 2019.

[21] EASA, “Easy Access Rules for Normal, Utility, Aerobatic and Commuter Category Aeroplanes (CS-23) (Initial issue),” Tech. rep., EASA, 2018.

[22] Barth, A., “Auslegung, Simulation, Bau und Flugerprobung eines unbemannten, elektrischen Hubschraubers mit kämmenden Rotoren für extreme Flughöhen,” *Dissertation*, 2020.

This work is licensed under the Creative Commons Attribution International License (CC BY). Copyright ©2021 by author(s).

[23] Barth, A., Spieß, C., Kondak, K., and Hajek, M., "Design, Analysis and Flight Testing of a High Altitude Synchropter UAV," *American Helicopter Society 74th Annual Forum, Phoenix, AZ*, 2018.

[24] Pflumm, T., Barth, A., Kondak, K., and Hajek, M., "Auslegung und Konstruktion eines Hauptrotorblattes für ein in extremen Flughöhen operierendes Drehflügel-UAV," *Deutscher Luft- und Raumfahrtkongress 2015*, edited by D. G. für Luft-und Raumfahrt Lilienthal-Oberth e.V., Deutsche Gesellschaft für Luft- und Raumfahrt - Lilienthal-Oberth e.V., Rostock, 2015, p. 11.

BIOGRAPHIES

Verena Heuschneider, M.Sc. is working as a Research Associate and PhD Candidate at the Institute of Helicopter Technology, Technical University of Munich, since March 2016. She graduated with an Aerospace Engineering Bachelor and Master at TUM with a Master´s Thesis on the topic of nonlinear stiffness and damping characteristics of a rotor blade attachment and their influence on helicopter ground resonance. Since January 2017 she was developing, designing and building the MERIT test rig until its initial operation in February 2021, continuing with blade sensor integration and strucural dynamic load investigations.

Florian Berghammer, M.Sc. is working as a Research Associate and PhD Candidate at the Institute of Helicopter Technology, Technical University of Munich, since November 2019. He graduated at TUM with a Master in Mechanical Engineering investigating critical eigenbehavior of the MERIT testrig at the Institute of Helicopter Technology for his Master's Thesis. In addition to supporting the installation and instrumentation of the test stand as a research associate, his focus lies on the integration of fiber optic sensors (FBG) into carbon fiber structures for operational load monitoring.

Tobias Pflumm, M.Sc. is working as a Research Associate and PhD Candidate at the Institute of Helicopter Technology, Technical University of Munich, since April 2015. He graduated at TUM with a Master in Aerospace, designing the AREA rotor blades for his Master's Thesis. Ever since that, multidisciplinary rotor blade design and its challenges dominate his research.

Prof. Dr.-Ing. Manfred Hajek is leading the Institute of Helicopter Technology at the Technical University of Munich since 2010. After graduating from TUM with a diploma and doctor´s degree in Aerospace Engineering at the Chair B for Mechanics in 1989, Prof. Hajek was employed in helicopter preliminary design. From 1998 onwards he lead the research and development department at Eurocopter Germany until he started as leader of the fuselage engineering department at Airbus in 2006. Especially through his lead in research projects between TUM and industrial partners Prof. Hajek has gained a wide spectrum of engineering knowledge within the aeronautical industry as well as many years of leadership experience. He is a Vertical Flight Society (VFS) educational member and was recently appointed corresponding member of the French Aerospace Academie.

This work is licensed under the Creative Commons Attribution International License (CC BY). Copyright ©2021 by author(s).

APPENDIX

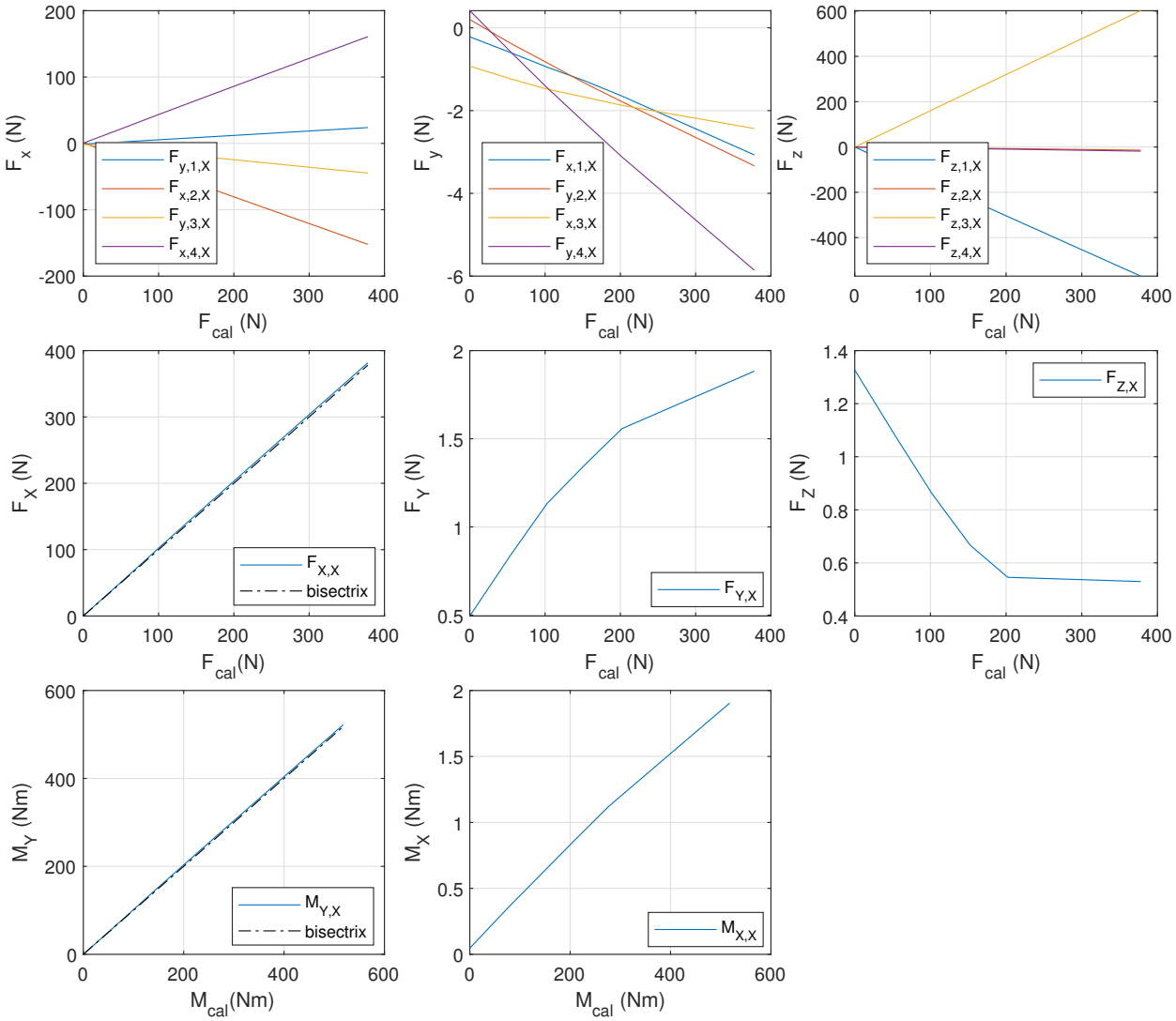

Fig. 24: Uncalibrated rotor forces and moments with transversal calibration load in global X direction

This work is licensed under the Creative Commons Attribution International License (CC BY). Copyright ©2021 by author(s).

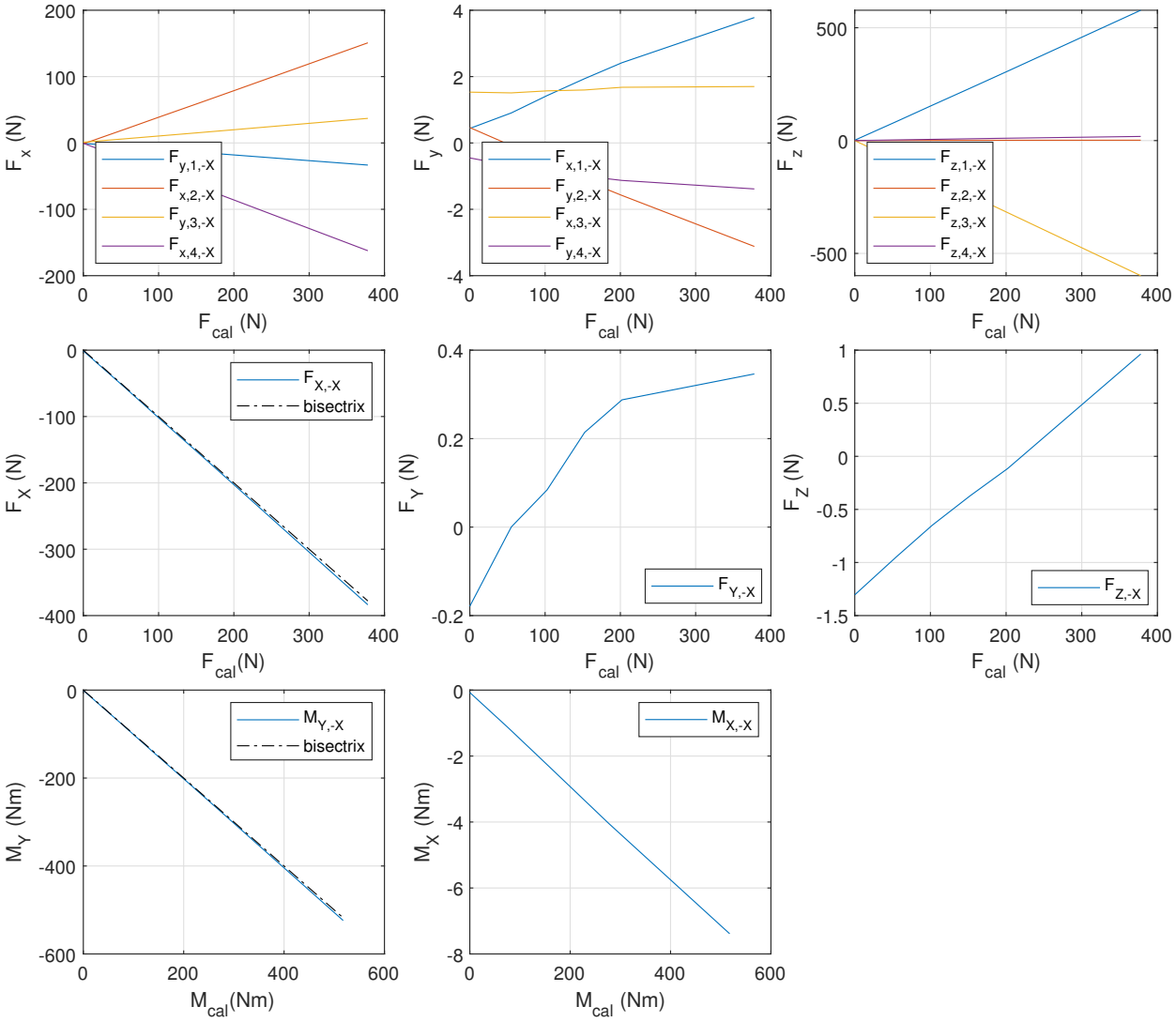

Fig. 25: Uncalibrated rotor forces and moments with transversal calibration load in global -X direction

This work is licensed under the Creative Commons Attribution International License (CC BY). Copyright ©2021 by author(s).

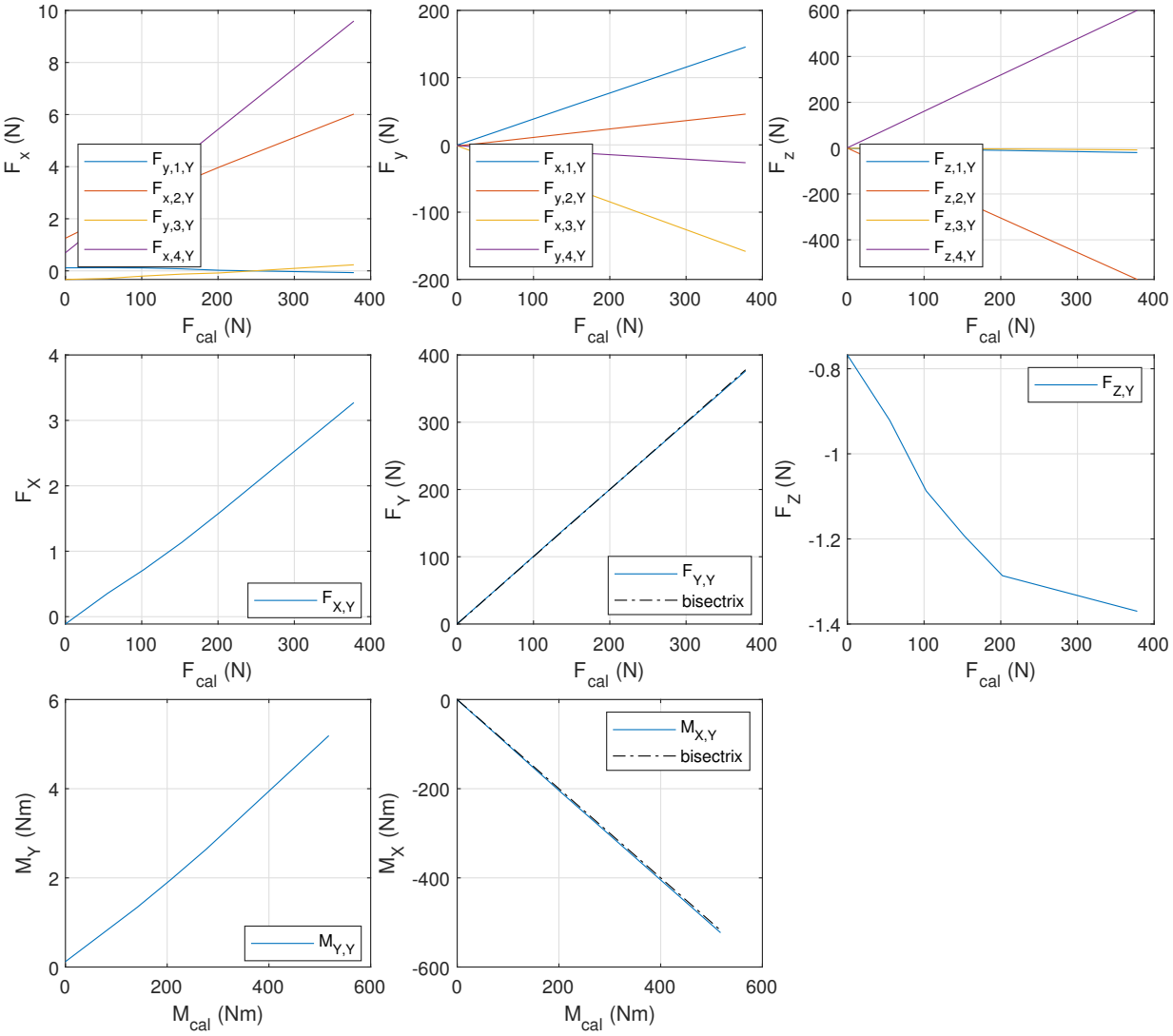

Fig. 26: Uncalibrated rotor forces and moments with transversal calibration load in global Y direction

This work is licensed under the Creative Commons Attribution International License (CC BY). Copyright ©2021 by author(s).

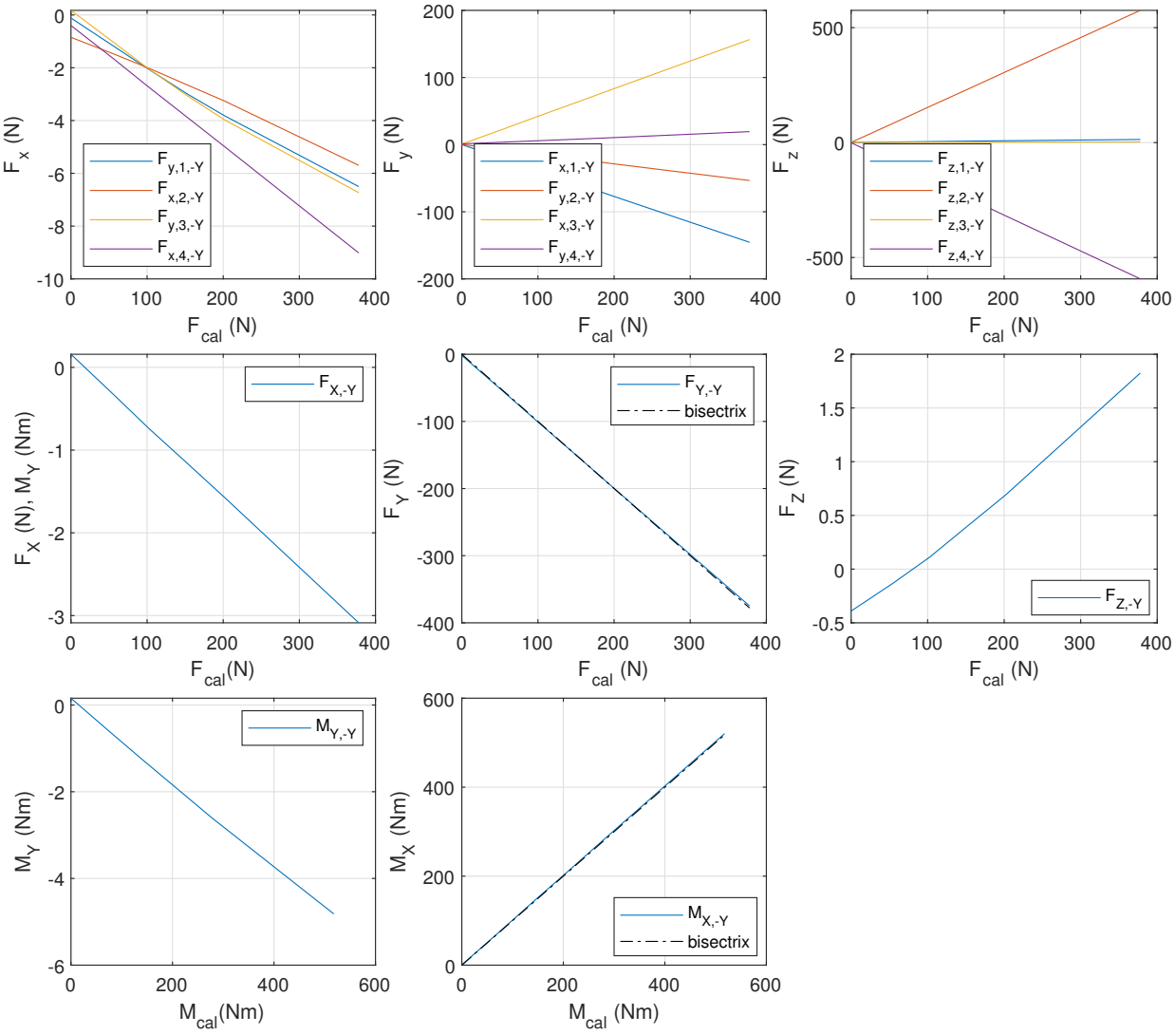

Fig. 27: Uncalibrated rotor forces and moments with transversal calibration load in global -Y direction

This work is licensed under the Creative Commons Attribution International License (CC BY). Copyright ©2021 by author(s).

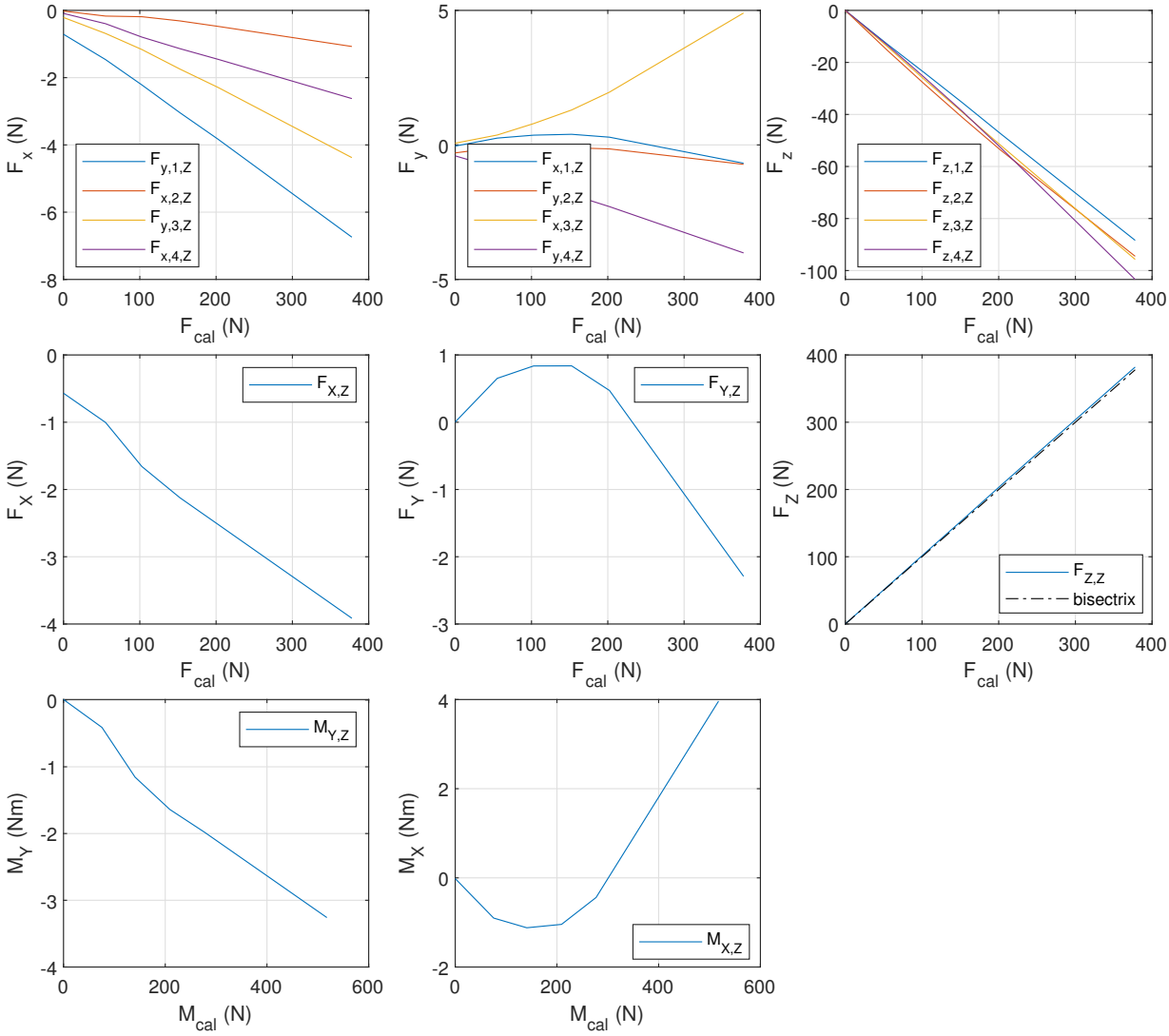

Fig. 28: Uncalibrated rotor forces and moments with axial calibration load in global Z direction

This work is licensed under the Creative Commons Attribution International License (CC BY). Copyright ©2021 by author(s).